

Processing of Integrated Gas Sensor Devices

(invited)

Lado Filipovic and Siegfried Selberherr, *Fellow, IEEE*

Abstract—The integration of gas sensor components into wearable electronics will provide individuals the ability to detect harmful chemicals and pollutants in the environment. The key to this integration is the development of processing techniques for the fabrication of sensor components which can be incorporated into the conventional CMOS fabrication sequence. This includes the etching required for the formation of a suspended membrane on top of which the microheater and sensing layer are placed and the deposition of the metal oxide sensing layer itself. Recently, spray pyrolysis has been investigated as a possible metal oxide deposition approach which is economical, easy to implement, and provides good step coverage for trench geometries. This work investigates wet chemical etching and plasma etching techniques for the generation of a suspended membrane and the spray pyrolysis and sputtering techniques for the deposition of a tin oxide gas sensing layer.

Keywords—gas sensor; tin oxide SnO_2 ; spray pyrolysis; sputter deposition; suspended membrane; thermal stress

I. INTRODUCTION

Our perception of the environment is partly shaped by the presence of various gases in our vicinity. The human nose serves as a natural sensor for hundreds of different odours, but fails when absolute gas concentrations or odourless gases require detection. The ability to detect these gases electrically is a topic of extensive research useful for a wide range of applications including environmental and safety monitoring. The feasibility to detect toxic and harmful gases in our environment through hand held and wearable devices is of particular significance triggering substantial research. In addition, fabrication and process controls, and laboratory analytics can be made more affordable with cheaper gas sensing equipment [1].

Currently, a variety of gas sensing principles are being implemented in industry, e.g. semiconductor, optical, thermal conductivity, quartz microbalance, catalytic, dielectric, electrochemical, and electrolyte sensors [1]. Recent discoveries in the use of metal oxides as gas sensing materials are at the forefront for enabling significant progress in moving away from bulky sensor architectures [1], [2], [3], [4], [5]. Two materials have been validated to exhibit all the properties required for a good gas sensing performance, namely zinc oxide (ZnO) [6], [7] and tin oxide (SnO_2) [8], [9], [10], while others such as indium tin oxide (ITO), In_2O_3 , CdO , ZnSnO_4 , NiO , etc. have also been widely studied [11]. These studies attempt to drive research towards the fabrication of cheap, small, and user-friendly devices with a high sensitivity, selectivity, and stability

with respect to the desired application. However, before a true integration of gas sensor components inside gadgets such as smart phones and wrist watches can be achieved, several challenges must be overcome:

- Until recently, gas sensor fabrication was not compatible with that of a conventional CMOS process sequence, which is essential for integration into hand-held electronics. An inexpensive technique which is compatible with the CMOS sequence is desired for the continued miniaturization of sensor components.
- Thin metal-oxide layers can only act as gas sensors when heated to temperatures between 250°C and 550°C , which means that a micro-hotplate must accompany each sensor. The integration of the hotplate and the sensor with the required analog and digital circuitry, as shown in Fig. 1, is necessary. Since metal oxides detect various gases, a sensor array is implemented in order to introduce selectivity in the sensor unit [12].

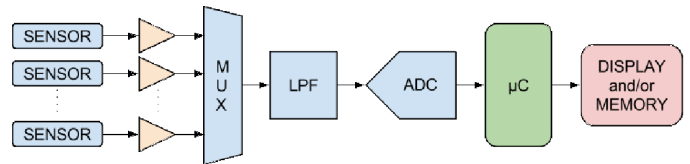


Fig. 1. Sensor unit showing a sensor array with interface electronics blocks, which include the amplifiers, multiplexer (MUX), low-pass filter (LPF), analog to digital converter (ADC), microcontroller (μC), and DISPLAY and/or MEMORY.

As already depicted in Fig. 1 the operation of a smart gas sensor implies the ability to detect a multitude of hazardous gases in the environment, for which multiple sensor circuits are required. The analog signals from these sensors is passed through an amplifier to a multiplexer. The output from the multiplexer is sent through a low-pass filter (LPF) and an analog to digital converter (ADC) before the signal can be analyzed with a microcontroller (μC) and eventually displayed or stored [13]. Although a major part of the electronics consists of analog and digital CMOS circuitry, the most complex component for integration and manufacturing is the sensor itself.

In this work, several aspects relating to the processing of a micromachined metal oxide gas sensor using a suspended membrane are discussed, mainly concentrating on the etching required to generate a suspended membrane and the deposition technique for the gas sensitive tin oxide layer.

A. Smart Gas Sensor Devices

Today's gas sensors are bulky devices, which are primarily dedicated to industrial applications. Since they are

(Invited) Manuscript received August XX, 2015;

L. Filipovic and S. Selberherr are with the Institute for Microelectronics, Technische Universität Wien, Gußhausstraße 27–29/E360, A-1040 Wien, Austria (Phone: +43-1-58801-36036, Fax: +43-1-58801-36099, e-mail: filipovic|selberherr@iue.tuwien.ac.at. 978-1-4799-8641-5/15/\$31.00 ©2015 IEEE.

not integrated in CMOS technology, they cannot fulfill the requirements for smart gas sensor applications in consumer electronics. A strategy to improve sensor performance is the implementation of very thin nanocrystalline films which have a high surface to volume ratio and thus a strong interaction with the surrounding gases. SnO₂ has been one of the most prominent sensing materials and a variety of gas sensor devices based on SnO₂ thin films has been realized so far [14], [15]. SnO₂ is a special material, as it has a low electrical resistance, a wide bandgap, and a high transparency in the visible spectrum [8]. It has also proven itself to be useful in many industries where an electric contact is required without obstructing photons from traveling through the optical active area. Tin oxide is also highly conductive due to high intrinsic defects.

A gas sensor which uses SnO₂ films with thicknesses of 50nm and 100nm has already been reported in [15]. The sensor itself operates on a micro-sized hotplate which heats the sensor locally to 250–400°C in order to detect humidity and harmful gases in the environment. The sensing mechanism of SnO₂ is related to the ionsorption of gas species over the surface, leading to charge transfer between the gas and surface molecules and changes in the electrical conductance [15].

B. Metal Oxide Sensor Operation

At increased temperatures, oxygen is adsorbed at the metal oxide surface by trapping electrons from the bulk material [16]. The result is the formation of a depletion layer at the surface and an overall decrease or increase in the metal oxide resistance, depending on whether the material is n-type or p-type, respectively. The introduction of a target gas in the atmosphere causes a reaction with the oxygen, removing it from the interface and reducing the band bending effect and thereby the overall resistance [17]. The thickness of the depletion layer is in the order of the Debye length, defined as

$$\lambda_D = \sqrt{\frac{\epsilon \cdot k_B \cdot T}{q^2 \cdot n_c}}, \quad (1)$$

where ϵ_0 is the free space permittivity, q is the elementary charge, and n_c is the carrier charge density.

Even though a good deal of effort has been aimed at understanding the gas sensing function of metal oxide materials, the exact chemistry of the sensing process is complex and not yet exhaustively understood [18]. The thin film can either be porous, where sensing occurs at the grain-level and between individual grains, or compact, where sensing occurs on the bulk material surface, as depicted in Fig. 2. A porous film is more complex to deposit when compared to a compact thin film, usually involving a sol-gel technique followed by a gelation step [18]. More recently, rheotaxial growth and vacuum oxidation was used to deposit porous films [19]. A compact metal oxide thin film can be deposited using a variety of techniques, including sputtering or spray pyrolysis which has recently gained traction due to its cost-effectiveness and integration within a standard CMOS processing sequence. This study concerns itself with the processes required to

manufacture a compact tin oxide gas sensor, deposited on a micromachined suspended membrane. The etching steps required for the generation of the suspended membrane and the deposition steps used for the tin oxide film growth are discussed in some detail in Section II and Section III.

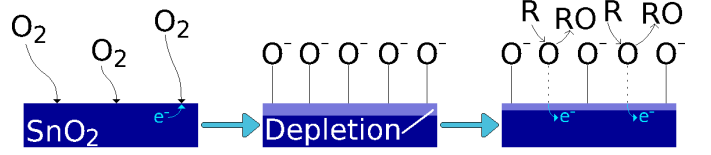


Fig. 2. Gas sensing function for a compact tin oxide film. The reaction occurs only at the top surface of the deposited tin oxide. The symbol R refers to a reducing gas.

C. Gas Sensor Geometry

The geometry of the sensor used in this study is depicted in Fig. 3. The membrane has an area of $200\mu\text{m} \times 200\mu\text{m}$ while the active sensor area is $100\mu\text{m} \times 100\mu\text{m}$. The beams connecting the membrane to the wafer are $100\mu\text{m}$ long and $20\mu\text{m}$ wide. The thicknesses of the membrane and the beams are $4\mu\text{m}$ with a microheater sandwiched between a $2\mu\text{m}$ SiO₂ layer at the bottom and a $2\mu\text{m}$ Si₃N₄ layer at the top. The aluminum electrodes and a 50nm thin tin oxide film are deposited on top of the Si₃N₄ layer above the microheater location.

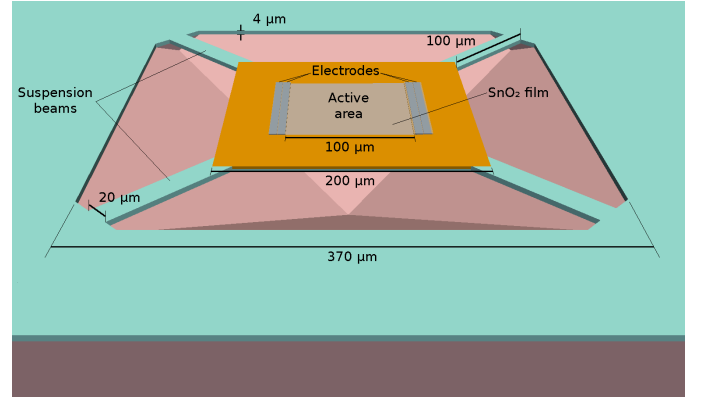


Fig. 3. Setup of the integrated gas sensor on top of a micromachined suspended membrane.

The top view of the sensing area is shown in Fig. 4, where four electrodes are evident. Four-electrode sensing is used for increased sensitivity and added accuracy, while eliminating the lead and contact resistances [20].

II. ETCHING FOR THE SENSOR MEMBRANE

For the fabrication of micromachined metal oxide gas sensors, two main membrane types are currently being investigated, the closed and suspended membranes [1]. For the production of both types, silicon is the starting material. For the closed membrane, the processing sequence requires anisotropic etching of silicon from the backside using etchants like

$$V_{KOH} = \begin{cases} \frac{-R_{100}(n_1 - n_2 - 2n_3) - R_{110}(n_2 - n_3) - 3R_{311}n_3}{2n_1} & \text{if } n_1 - n_2 - 2n_3 > 0 \\ \frac{R_{111}(n_1 - n_2 - 2n_3) - 2R_{110}(n_2 - n_3) - 3R_{311}(n_1 - n_2)}{2n_1} & \text{otherwise.} \end{cases} \quad (2)$$

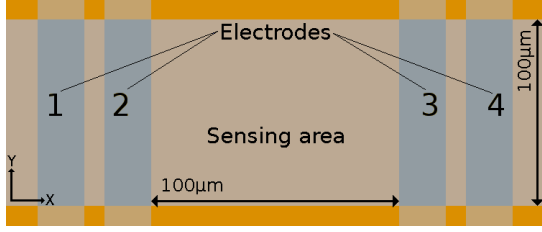


Fig. 4. Top view of the electrode locations on the substrate with the sensing area (SnO_2) is deposited on top of four electrodes. The sensing area is $100\mu\text{m} \times 100\mu\text{m}$.

potassium hydroxide (KOH) or ethylenediamine-pyrocatechol-pyrazine (EDP) with the use of silicon nitride or silicon oxide as etch stop layers [21]. This process results in membranes with thicknesses between $1\mu\text{m}$ and $2\mu\text{m}$ [22]. An alternate process using porous silicon nitride can generate thicknesses between $25\mu\text{m}$ and $30\mu\text{m}$ [23].

In this work attention is given to the suspended membrane gas sensor, because it is fully processed on the front side of the wafer, making it fully compatible with CMOS fabrication [24]. The membrane is formed using photolithographic methods to selectively expose silicon and etching through the silicon wafer, until a well is created below the eventual membrane. Once again, the etching can be performed using chemical etchants such as KOH [25] or EDP [26]. An alternative to the cost-intensive chemical etching is etching in a plasma, likewise using openings in the silicon nitride or silicon oxide membrane. In this section, simulation models for KOH and plasma etching are used to generate a suspended membrane structure and the viabilities of the two methods are discussed.

A. Chemical KOH Etching

The modeling of the anisotropic etching of silicon using KOH is described by Radjenović in [27] and its implementation within the level set method is detailed by Ertl in [28]. The surface velocities during etching depends on the crystallographic orientation of the surface, resulting in faster etching times for some directions and slower for others, which is ideal for a suspended membrane structure. Using the models given in [27] and [28], the surface velocity can be approximated by (2), where R_{100} , R_{110} , R_{111} , and R_{311} correspond to the etch rates in the crystallographic directions $\langle 100 \rangle$, $\langle 110 \rangle$, $\langle 111 \rangle$, and $\langle 311 \rangle$, respectively. The surface normal vector is given by $\vec{n} = (n_1, n_2, n_3)$, where n_1 , n_2 , and n_3 correspond to the directions $[100]$, $[010]$, and $[001]$, respectively. This model only considers the case where $1 \geq n_3 \geq n_2 \geq n_1 \geq 0$ and for the model used, the rates are $R_{100} = 0.797\mu\text{m}/\text{min}$, $R_{110} = 1.455\mu\text{m}/\text{min}$, $R_{111} = 0.005\mu\text{m}/\text{min}$, and $R_{311} = 1.436\mu\text{m}/\text{min}$.

Using a KOH concentration of 30% and a temperature of 70°C , as suggested in [25], the suspended membrane with a geometry shown in Fig. 3 is generated. The structure resulting after a 150-minute etch is depicted in Fig. 5, where a well with a $100\mu\text{m}$ depth is generated below the membrane. Although

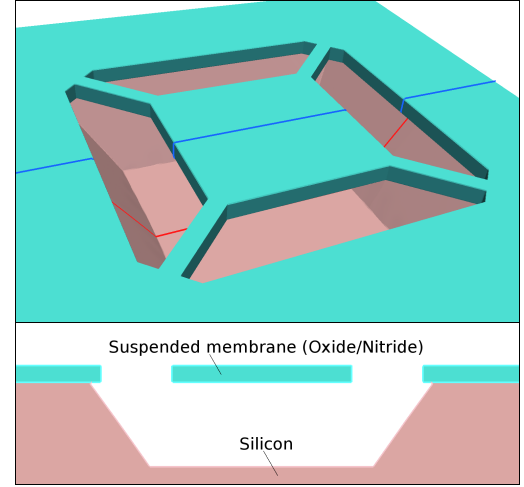


Fig. 5. Suspended membrane structure after a chemical etch using a 30% KOH mixture at 70°C .

the KOH etched structure displays a clean geometry and a well which prevents undesirable lateral etching, the process is very corrosive. KOH heavily attacks the aluminum metalization films making the process not fully compatible for CMOS fabrication [29]. This means that additional care is required during the etching process to ensure proper isolation of layers which may be corroded by KOH.

B. Plasma Etching

An alternative to the corrosive chemical KOH etching is etching in a plasma environment, usually using SF_6 gas to selectively remove silicon, while the oxide mask is etched at a rate 100 times slower. A description of the etching physics and its modeling is given in [30] and [31], respectively. The presented model is implemented in an in-house level set simulator and a simulation on the structure geometry from Fig. 3 is carried out. The etch rate of silicon is influenced by the fluorine and ions present in the plasma chamber as described in [31]

$$V_{plasma} = \frac{1}{\rho_{Si}} \left(\frac{k\sigma_{Si}\theta_F}{4} + Y_p\Gamma_i + Y_{Si}\Gamma_i\theta_F \right), \quad (3)$$

where ρ_{Si} is the Si density, $k\sigma_{Si}$ is the chemical etch reaction rate constant, Y_p is the physical sputtering yield, Y_{Si} is the

ion-enhanced etch yield, Γ_i is the total ion flux, and θ_F is the fluorine surface coverage, given by

$$\theta_F = \frac{1}{1 + \frac{k\sigma_{Si}}{\gamma_F\Gamma_F} + \frac{2Y_i\Gamma_i}{\gamma_F\Gamma_F}}, \quad (4)$$

where γ_F is the initial fluorine sticking coefficient. Using a fluorine flux of $1 \times 10^{19} \text{cm}^{-2}\text{s}^{-1}$ and disregarding any ion enhancement, a 300 second etch results in the profile shown in Fig. 6.

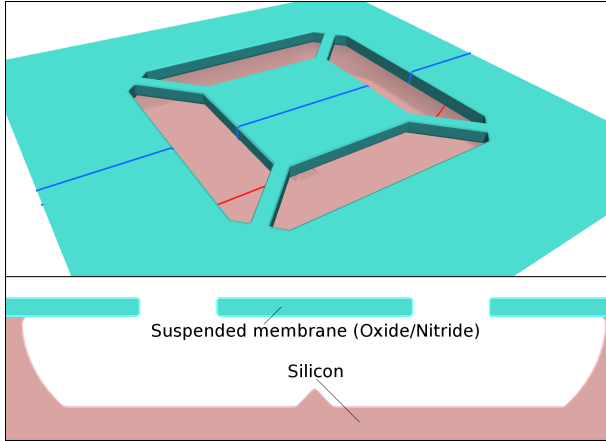


Fig. 6. Suspended membrane structure after a SF_6 plasma etch for a duration of 300 seconds.

Although plasma etching is compatible with the CMOS process, there are still hurdles which must be overcome. In order to ensure a complete etch below the suspended membrane, a large isotropic etch component is required. However, due to the inherent isotropy of plasma etching, lateral etching proceeds in all directions, resulting in a wide well, as can be seen in Fig. 6. In order to limit the lateral etching, blocking layers of oxide or nitride may be used adding complexity and expense to the membrane formation.

C. Stress in the Suspended Membrane

The stress in the semiconductor membrane is a combination of the residual stresses in the layers which make up the complete membrane. The control of the residual stress in single layers and especially multilayer systems, such as the micromachined membrane presented here, is crucial for stability [32]. Typical values for the residual stress in Si_3N_4 (1GPa [33]) and SiO_2 (-320MPa [34]) films are applied and the stress distribution in the full membrane with beams is simulated in a finite element environment.

The resulting stress through the active area of the KOH etched membrane is plotted in Fig. 7 and the one-dimensional stress through the middle of the membrane for both etch types is shown in Fig. 8. The resulting average stress through the active region for both instances is found to be approximately 300MPa. However, due to the added lateral etch in the plasma membrane, the vertical displacement is found to be $8\mu\text{m}$ compared to a displacement of $5\mu\text{m}$ for the KOH membrane.

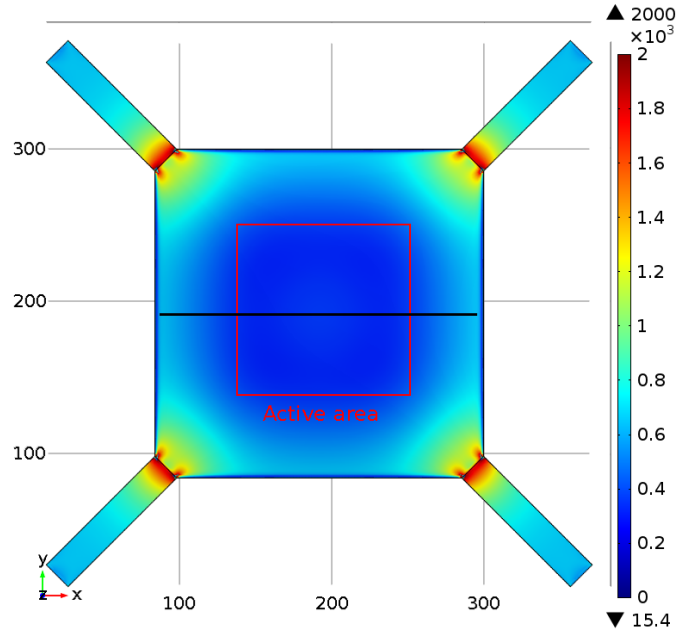


Fig. 7. Stress distribution through the sensor membrane, when 1GPa and -320MPa residual stresses are observed in the Si_3N_4 and SiO_2 layers, respectively.

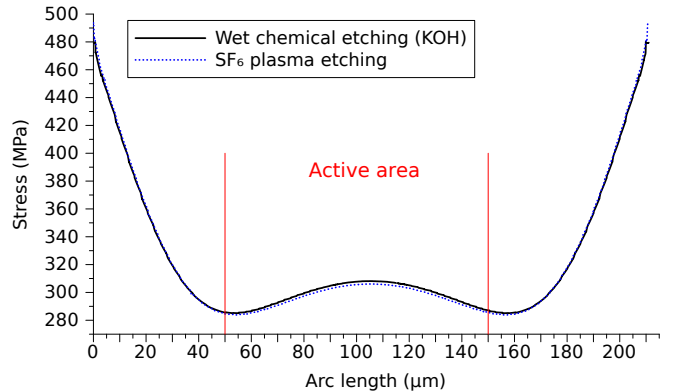


Fig. 8. Stress distribution through the middle of the sensor structure as depicted with a solid black line in Fig. 7.

III. SENSING LAYER DEPOSITION

The second critical processing step for the fabrication of a suspended membrane, micromachined gas sensor is the deposition of a metal oxide layer to act as the sensing element. Deposition can proceed in a variety of ways, including chemical vapor deposition [35], sputtering [36], pulsed-laser deposition [37], sol-gel process [38], rheotaxial growth and vacuum oxidation [19], and spray pyrolysis [8]. Sputtering and spray pyrolysis are methods which are quite straight forward to implement within the CMOS sequence.

A. Sputter Deposition of Tin Oxide

A model for sputter deposition given in [39] is implemented in an in-house level set simulator in order to model the growth of tin oxide. The model considers a yield function F which depends on the impact angle of a depositing particle in relation to the surface normal θ as given by

$$F(\theta) = (1 + 4 \cdot \sin^2\theta) \cos\theta. \quad (5)$$

A simulation of sputter deposition was carried out on a typical four-contact sensor structure with a complex step geometry [9] and the result is shown in Fig. 9. As can be observed in Fig. 9 the tin oxide thickness is not uniform throughout. This means that a flat wafer geometry should be used when sputter deposition is performed, causing an increased complexity in the deposition of the metal electrodes. The stress built up during the sputter deposition at approximately 70°C with a low oxygen content in the sputtering gas is found to be about 200MPa [36].

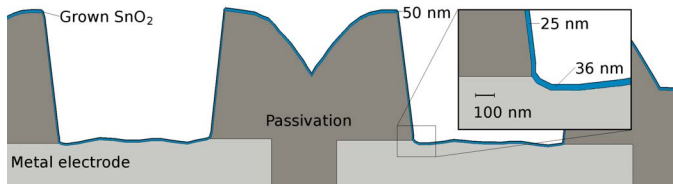


Fig. 9. Image showing the simulated deposited SnO₂ film as a result of sputter deposition. The deposition rate depends on the surface normals, resulting in a non-uniform film thickness throughout.

B. Spray Pyrolysis Deposition of Tin Oxide

A model for the spray pyrolysis deposition of tin oxide is developed and calibrated with experimental data, which shows a linear dependence on spray time and a logarithmic dependence on wafer temperature for the growth rate of the deposited SnO₂ layer. A good agreement for the deposited SnO₂ thickness, in μm , is given by the Arrhenius expression

$$d_{\text{SnO}_2}(t, T) = A_1 t e^{(-E/k_B T)}, \quad (6)$$

where $A_1 = 3.1 \mu\text{m}/\text{sec}$, t is the time in seconds, T is the temperature in Kelvin, and E is 0.427eV. The growth model given in (6) relates the thickness of the deposited material to the applied time and temperature. However, this representation is only valid, when no complex geometries such as deep wells, trenches, and step structures are present. In order to model deposition on a deep well structure, more than a single deposition rate have to be considered.

This deposition technique proceeds by spraying small depositant droplets in the direction of the heated wafer. As the droplets reach the wafer vicinity, they evaporate resulting in the deposition of the depositant in vapour form. The simulation, therefore, requires a non-linear model analogous to CVD which is implemented in the level set framework using Monte Carlo methods and ray tracing [40]. As the simulation is initiated, multiple particles are generated in the simulation space with an average direction perpendicular to and moving towards the wafer. For the spray pyrolysis deposition process it was found that a sticking coefficient of 0.01 gives the best fit

to experimental data and was therefore used for the model. The motion of reflected or re-emitted particles is then tracked with their sticking probability reduced after each surface impact.

Using the given equation and the presented model, a simulation was performed for 30 seconds at 400°C on the full geometry of a gas sensing electrode with the result shown in Fig. 10. The film has an evenly distributed thickness of approximately 50nm independent of the surface direction, as expected from the measured thickness noted in experimental observations [40].

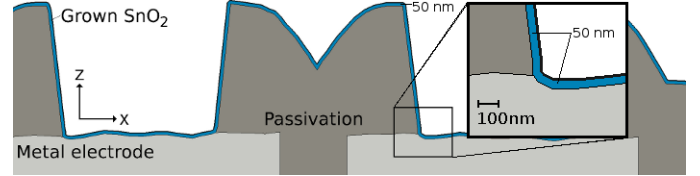


Fig. 10. Image showing the simulated deposited SnO₂ film as a result of spray pyrolysis deposition. The deposition is performed with the heated substrate at a temperature $T=400^\circ\text{C}$ for a time $t=30\text{s}$.

Due to the temperature used during deposition, the intrinsic stress is not a major concern, while the thermal stress resulting due to cooling from the 400°C deposition temperature plays a larger role. A finite element simulation is performed on cooling the device from the deposition temperature to room temperature resulting in a stress of 380MPa. Although the stress in the sputtered film is slightly lower, the spray pyrolysis method is much more cost effective.

IV. CONCLUSION

An analysis of the processes required for the fabrication of a tin oxide micromachined gas sensor device using a suspended membrane was performed. One critical manufacturing step for the generation of the device is the etching of silicon through openings in the nitride/oxide mask in order to generate the suspended membrane. This step can be performed using chemical wet etching with KOH as the etchant or etching in a SF₆ plasma. Models for both methods have been implemented in a level set framework and the feasibility of generating the desired architecture is presented. The KOH-etched membrane displays a much cleaner well under the membrane; however, the process is very corrosive and can lead to damage of the metal layers. Plasma etching, on the other hand, is compatible to the CMOS fabrication sequence; however, the extreme amount of lateral etching results in a very wide well, causing a larger displacement in the active membrane region.

The second critical step for the generation of an integrated smart sensor device is the deposition of a thin metal oxide layer. This study examined sputtering and spray pyrolysis as potential fabrication techniques to deposit a 50nm tin oxide layer. Sputtering resulted in a layer with a thickness dependent on the surface normal and a 200MPa of intrinsic stress. However, spray pyrolysis, an inexpensive and easily implementable deposition technique, led to the formation of a very uniform thin film around corners and step structures with a thermo-mechanical stress of 380MPa, due to the 400°C temperature required for deposition.

REFERENCES

- [1] I. Simon, N. Bârsan, M. Bauer, and U. Weimar, *Sensors and Actuators B: Chemical*, vol. 73, no. 1, pp. 1–26, 2001.
- [2] N. Barsan, D. Koziej, and U. Weimar, *Sensors and Actuators B: Chemical*, vol. 121, no. 1, pp. 18–35, 2007.
- [3] C. Wang, L. Yin, L. Zhang, D. Xiang, and R. Gao, *Sensors*, vol. 10, no. 3, pp. 2088–2106, 2010.
- [4] C. Pijolat, *Chemical Sensors and Biosensors*, pp. 93–125, 2012.
- [5] G. Korotcenkov, “Metal oxide-based nanostructures,” in *Handbook of Gas Sensor Materials*. Springer, 2014, pp. 47–71.
- [6] M. Ortel, Y. S. Trostyanskaya, and V. Wagner, *Solid-State Electronics*, vol. 86, pp. 22–26, 2013.
- [7] M. Prasad, V. Sahula, and V. Khanna, *IEEE Transactions on Semiconductor Manufacturing*, vol. 26, no. 2, pp. 233–241, 2013.
- [8] G. Patil, D. Kajale, V. Gaikwad, and G. Jain, *ISRN Nanotechnology*, vol. 2012, 2012.
- [9] G. Mutinati, E. Brunet, S. Steinhauer, A. Köck, J. Teva, J. Kraft, J. Siegert, F. Schrank, and E. Bertagnoli, *Procedia Engineering*, vol. 47, pp. 490–493, 2012.
- [10] E. Brunet, T. Maier, G. Mutinati, S. Steinhauer, A. Köck, C. Gspan, and W. Grogger, *Sensors and Actuators B: Chemical*, vol. 165, no. 1, pp. 110–118, 2012.
- [11] A. Bouaoud, A. Rmili, F. Ouachtari, A. Louardi, T. Chtouki, B. Elidrissi, and H. Erguig, *Materials Chemistry and Physics*, vol. 137, no. 3, pp. 843–847, 2013.
- [12] U. Hofer, H. Böttner, A. Felske, G. Kühner, K. Steiner, and G. Sulz, *Sensors and Actuators B: Chemical*, vol. 44, no. 1, pp. 429–433, 1997.
- [13] J. W. Gardner, P. K. Guha, F. Udrea, and J. A. Covington, *IEEE Sensors Journal*, vol. 10, no. 12, pp. 1833–1848, 2010.
- [14] W. Göpel and K. Schierbaum, *Sensors and Actuators B: Chemical*, vol. 26–27, pp. 1–12, 1995.
- [15] A. Tischner, T. Maier, C. Stepper, and A. Köck, *Sensors and Actuators B: Chemical*, vol. 134, no. 2, pp. 796–802, 2008.
- [16] L. Filipovic and S. Selberherr, *Sensors*, vol. 15, no. 4, pp. 7206–7227, 2015.
- [17] N. Barsan and U. Weimar, *Tagungsband*, pp. 618–621, 2012.
- [18] M. Tiemann, *Chemistry-A European Journal*, vol. 13, no. 30, pp. 8376–8388, 2007.
- [19] M. Kwoka and M. Krzywiecki, *Materials Letters*, vol. 154, pp. 1–4, 2015.
- [20] H. Liu, J. Kameoka, D. A. Czaplowski, and H. Craighead, *Nano Letters*, vol. 4, no. 4, pp. 671–675, 2004.
- [21] B.-U. Moon, J.-M. Lee, C.-H. Shim, M.-B. Lee, J.-H. Lee, D.-D. Lee, and J.-H. Lee, *Sensors and Actuators B: Chemical*, vol. 108, no. 1, pp. 271–277, 2005.
- [22] A. Götz, I. Gracia, C. Cané, E. Lora-Tamayo, M. Horrillo, J. Getino, C. Garcia, and J. Gutiérrez, *Sensors and Actuators B: Chemical*, vol. 44, no. 1, pp. 483–487, 1997.
- [23] P. Maccagnani, L. Dori, and P. Negrini, “Thermo-insulated microstructures based on thick porous silicon membranes,” in *Proceedings of the 13th European Conference on Solid-State Transducers*, 1999, pp. 12–15.
- [24] L.-y. Sheng, Z. Tang, J. Wu, P. C. Chan, and J. K. Sin, *Sensors and Actuators B: Chemical*, vol. 49, no. 1, pp. 81–87, 1998.
- [25] K. Sato, M. Shikida, Y. Matsushima, T. Yamashiro, K. Asaumi, Y. Iriye, and M. Yamamoto, *Sensors and Actuators A: Physical*, vol. 64, no. 1, pp. 87–93, 1998.
- [26] H. Seidel, L. Csepregi, A. Heuberger, and H. Baumgärtel, *Journal of the Electrochemical Society*, vol. 137, no. 11, pp. 3612–3626, 1990.
- [27] B. Radjenović and M. Radmilović-Radjenović, *Thin Solid Films*, vol. 517, no. 14, pp. 4233–4237, 2009.
- [28] O. Ertl, “Numerical methods for topography simulation,” Dissertation, Technischen Universität Wien, Fakultät für Elektrotechnik und Informationstechnik, May 2010, <http://www.iue.tuwien.ac.at/phd/ertl/>.
- [29] U. Munch, N. Schneeberger, O. Paul, H. Baltes, and E. Doering, “Thin film front protection of CMOS wafers against KOH,” in *Micromachining and Microfabrication*. International Society for Optics and Photonics, 1998, pp. 124–133.
- [30] S. Gomez, R. Jun Belen, M. Kiehlbauch, and E. S. Aydil, *Journal of Vacuum Science Technology*, vol. 22, pp. 606–615, 2004.
- [31] R. J. Belen, S. Gomez, M. Kiehlbauch, D. Cooperberg, and E. S. Aydil, *Journal of Vacuum Science & Technology A: Vacuum, Surfaces, and Films*, vol. 23, no. 1, pp. 99–113, 2005.
- [32] H. M. Low, M. S. Tse, and M. M. Chiu, “Thermal induced stress on the membrane in integrated gas sensor with micro-heater,” in *Proceedings of the IEEE Electron Devices Meeting*, 1998, pp. 140–143.
- [33] E. Irene, *Journal of Electronic Materials*, vol. 5, no. 3, pp. 287–298, 1976.
- [34] H. Leplan, J. Robic, and Y. Pauleau, *Journal of Applied Physics*, vol. 79, no. 9, pp. 6926–6931, 1996.
- [35] I. Volintiru, A. de Graaf, J. Van Deelen, and P. Poodt, *Thin Solid Films*, vol. 519, no. 19, pp. 6258–6263, 2011.
- [36] J. Boltz, D. Koehl, and M. Wuttig, *Surface and Coatings Technology*, vol. 205, no. 7, pp. 2455–2460, 2010.
- [37] S. Sinha, R. Bhattacharya, S. Ray, and I. Manna, *Materials Letters*, vol. 65, no. 2, pp. 146–149, 2011.
- [38] D. M. Carvalho, J. L. Maciel Jr, L. P. Ravaro, R. E. Garcia, V. G. Ferreira, and L. V. Scalvi, *Journal of Sol-Gel Science and Technology*, vol. 55, no. 3, pp. 385–393, 2010.
- [39] D. Adalsteinsson and J. Sethian, *Journal of Computational Physics*, vol. 120, no. 1, pp. 128–144, 1995.
- [40] L. Filipovic, S. Selberherr, G. Mutinati, E. Brunet, S. Steinhauer, A. Köck, J. Teva, J. Kraft, J. Siegert, F. Schrank, C. Gspan, and W. Grogger, *IEEE Transactions on Semiconductor Manufacturing*, vol. 27, no. 2, pp. 269–277, May 2014.



Lado Filipovic studied electrical engineering at Carleton University in Ottawa, ON, Canada, where he obtained his Bachelors in Engineering and Masters in Applied Sciences degrees in 2006 and 2009, respectively. In 2010 he joined the Institute for Microelectronics at the TU Wien, lead by Siegfried Selberherr. There, he obtained his doctoral degree in technical sciences in 2012. The main focus of his postdoctoral work is modeling processing techniques and the effects of process variability on semiconductor devices, mainly dealing with smart gas sensors, through silicon vias, and interconnect structures.



Siegfried Selberherr (M79-SM84-F93) was born in Klosterneuburg, Austria, in 1955. He received the degree of Diplomingenieur in electrical engineering and the doctoral degree in technical sciences from the Technische Universität Wien in 1978 and 1981, respectively. Dr. Selberherr has been holding the *venia docendi* on computer-aided design since 1984. Since 1988 he has been the Chair Professor of the Institut für Mikroelektronik. From 1998 to 2005 he served as Dean of the Fakultät für Elektrotechnik und Informationstechnik. Prof. Selberherr published more than 350 papers in journals and books, where more than 100 appeared in Transactions of the IEEE. He and his research teams achieved more than 1000 articles in conference proceedings of which more than 150 have been with an invited talk. Prof. Selberherr authored two books and co-edited 30 volumes, and he supervised, so far, more than 100 dissertations. His current research interests are modeling and simulation of problems for microelectronics engineering.